The Hydrophobic Pocket Contributes to the Structural Stability of the N-Terminal Coiled Coil of HIV gp41 but Is Not Required for Six-Helix Bundle Formation

John J. Dwyer, Aisha Hasan, Karen L. Wilson, Jonathan M. White, Thomas J. Matthews, and Mary K. Delmedico*

Trimeris, Inc., 3518 Westgate Drive, Durham, North Carolina 27707

Received December 3, 2002; Revised Manuscript Received February 26, 2003

ABSTRACT: In models of HIV fusion, the glycoprotein gp41 is thought to form a six-helix bundle during viral fusion with the target cell. This bundle is comprised of three helical regions (from the heptad repeat 2, or HR2, region of gp41) bound to an inner, trimeric, coiled-coil core (from the HR1 region). Although much has been learned about the structure and thermodynamics of this complex, the energetics of the isolated HR1 self-associated oligomer remain largely unknown. By systematically studying self-association through a series of truncations based on a 51-mer HR1 peptide (T865), we have identified amino acid segments which contribute significantly to the stability of the oligomeric HR1 complex. Biophysical characterization of C-terminal truncations of T865 identifies a 10−15-amino acid region that is essential for HR1 oligomerization. This region coincides with a hydrophobic pocket that provides important contacts for the interaction of HR2 helices. Complete removal of this pocket abolishes HR1 oligomerization. Despite the dramatic reduction in stability, the monomeric HR1 peptides are still able to form stable six-helix bundles in the presence of HR2 peptides. Truncations on the N-terminal side of T865 have little effect on oligomerization but significantly reduce the stability of the HR1−HR2 six-helix bundle. Unlike the HR2 binding site, which extends along a hydrophobic groove on the HR1 oligomer, the residues that are critical for HR1 oligomerization are concentrated in a 10−15-amino acid region. These results demonstrate that there are localizations of binding energy, or "hot spots", in the self-association of peptides derived from the HR1 region of gp41.

The envelope glycoprotein complex (gp120−gp41) of human immunodeficiency virus type 1 (HIV-1)[1] has important functions in the early stages of viral infection (*1*, *2*). After viral attachment to cells, this glycoprotein is thought to undergo a series of complex conformational rearrangements which ultimately result in the fusion between the cellular and viral membranes (*3*). Understanding how these structural changes facilitate fusion has been the subject of intense study in recent years because this glycoprotein appears to be an attractive target for blocking viral entry (*4*). A peptide inhibitor of viral fusion known as enfuvirtide (T20), currently in Phase III clinical trials for the treatment of HIV, is thought to reduce viral infection by interfering with conformational changes in the envelope gp41 subunit that is required for formation of a fusion-active state (*5*−*7*).

Mounting evidence supports the model that prior to fusion, the viral gp41 fusion protein exists in a nonfusogenic or native state, for which little structural information is available. The transition to a fusogenic state begins with gp120 interacting with CD4 and cellular coreceptors and altering its association with gp41 (*4*). This allows the fusion peptide sequence, located on the amino terminus of gp41, to insert into the membrane of the target cell. The gp41 ectodomain then undergoes a series of conformational changes to form the fusion-active, or fusogenic, state. Several recent crystallographic structures of peptides derived from regions of gp41 have elucidated the proposed structure of the fusogenic state (*3*, *8*, *9*). The structures of these complexes support the idea that regions on the N-terminal side of the fusion protein (HR1), near the fusion peptide, form a trimeric coiled-coil core and that regions on the carboxy-terminal side (HR2), closer to the transmembrane domain, interact with grooves on the coiled-coil structure to form a six-helix bundle complex. Despite the wealth of structural data, little is currently known about the structure of either HR1 or HR2 in the nonfusogenic, or native, state.

The coiled-coil nature of the N- and C-terminal domains of HIV gp41 (*10*, *11*) and other viruses (*12*) had been predicted on the basis of the identification of heptad repeat (HR) regions. The heptad repeat is characterized by a preference for hydrophobic amino acids at the "a" and "d" positions of the heptad, and hydrophilic residues at the "b", "c", and "e"−"g" positions. This pattern places hydrophobic side chains along one face of an α-helix upon folding which can interact with other helicies to form the coiled-coil structural motif. Studies on other coiled-coil structures, such as GCN4, have demonstrated that the core "a" and "d" residues are important for both the stability and oligomeric specificity of the coiled-coil structure (*13*). Although it has been noted that positions other than "a" and "d" can potentially affect oligomeric states (*14*), the contributions by these positions in the heptad to the structural stability of the coiled coil are not well understood.

* To whom correspondence should be addressed. Phone: (919) 419-6050. Fax: (919) 408-5191. E-mail: mdelmedico@trimeris.com.

[1] Abbreviations: HR, heptad repeat; HIV, human immunodeficiency virus; RSV, respiratory syncitial virus; CD, circular dichroism; XLA, analytical ultracentrifugation; LS, light scattering.

10.1021/bi027283n CCC: $25.00
Published on Web 04/09/2003

A prominent feature noted in the structures of the gp41 six-helix bundle is a deep hydrophobic groove or "pocket" on the HR1 trimeric coiled coil (*15*). Residues from the HR2 region make numerous contacts in this region, and it has been shown that changes in this area have a significant impact on HR2 binding to the HR1 core (*15*). Although the fusion inhibitor T20 is not thought to interact with this area, other peptides known to interact with the pocket exhibit antiviral activity (*16*, *17*).

The hydrophobic pocket clearly provides an important set of contacts for the binding of HR2 regions to the oligomeric HR1 core. In this report, we have demonstrated that residues in the vicinity of this pocket also contribute significantly to the stability of the self-associated HR1 structure while other areas are much less important. These results highlight the fact that not all segments of the inner HR1 coiled coil contribute equally to structural stability, but rather there are "hot spots" of localized binding energy in the self-associated complex.

The structure of the HR1−HR2 complex from respiratory syncitial virus (RSV) (*18*), together with the results from our previous study (*19*), suggests that the hydrophobic pocket may be a conserved region for stabilizing the oligomeric inner core. Agents that prevent HR1 oligomerization may also prove to be attractive targets for preventing viral fusion as they might work at an earlier stage of the fusion process than inhibitors currently under development.

EXPERIMENTAL PROCEDURES

Preparation of Peptide Samples. Peptides were synthesized as previously reported (*19*) and purified to >90% purity. Peptide identity was confirmed by mass spectrometry. Lyophilized peptide samples were resuspended in dH_2O to a concentration of approximately 1 mg/mL except for T649 which was resuspended in phosphate buffer [50 mM KPO_4 and 100 mM NaCl (pH 7.0)]. Concentrations were determined using the method of Edelhoch (*20*) except for that of peptide T1847, which was determined by amino acid analysis (Biosynthesis Inc., Lewisville, TX). Each peptide was then diluted to the appropriate concentration using phosphate buffer.

Circular Dichroism Spectroscopy. Circular dichroism (CD) spectra were obtained using an AVIV Associates 62DS spectrometer equipped with a thermoelectric temperature controller. Spectra were obtained in 0.1, 0.5, or 1.0 cm quartz cells at 1 °C with 0.5 nm steps from 200 to 260 nm, a 1.5 nm bandwidth, and an averaging time of 4 s/step. After the spectrum of the buffer was subtracted, peptide spectra were smoothed using a third-order least-squares polynomial fit with a conservative (5−10-point) window size to give random residuals. Raw ellipticity values were converted to mean residue ellipticity using standard methods (*21*). Percent helicity values were calculated using single-value decomposition with a basis set of 33 protein spectra (*22*). Thermal stability measurements were performed at 222 nm with 2 °C steps from 1 to 97 °C, and an averaging time of 16 s/step. The reported T_m value is the temperature corresponding to the maximum value of the first derivative of the thermal transition. Helicity and T_m values are the averages of at least two independent measurements.

Analytical Ultracentrifugation. Sedimentation equilibrium experiments were performed on a Beckman Optima XL-A analytical ultracentrifuge at 4 °C. Six-channel cells (optical path length of 12 mm) were used with either an An-50 or An-60 titanium rotor. The cells were scanned using a step size of 0.001 cm, and data points were averaged over 10 replicates. Samples were initially scanned at 3000 rpm to identify appropriate wavelengths for data collection. The absorbances obtained at 3000 rpm were compared to the absorbances at 35 000 rpm to ensure that the peptides remained in solution over the course of the experiment. For reported molecular masses, there was no significant decrease in absorbance due to the sedimentation of very high molecular mass aggregates. Data were collected at 18 000, 22 000, and 35 000 rpm and at three wavelengths (typically 235, 240, and 280 nm).

Weight-averaged molecular masses were obtained by fitting each data file individually using a single-ideal species model in the Beckman-Origin software (version 3.78 for Windows) and averaging the molecular masses from all data sets. The solvent density ($\rho = 1.01837$) and partial specific volumes were calculated using the program SEDNTERP (version 1.05) (*23*). For equal-molar peptide mixtures, the average partial specific volume of each peptide was used. Poor fits to the single-ideal species model (systematic residuals) and molecular masses which varied with rotor speed (more than 10%) were considered a diagnostic for aggregation or higher-order association.

The program NONLIN (version 1.06) (*24*) was used to simultaneously fit sedimentation data from different loading concentrations, speeds, and wavelengths (up to 15 separate data files) to determine the reduced molecular mass for the self-associating peptides. Data from different wavelengths were normalized using Beer's law, and data from different speeds were scaled using speed factors described in NONLIN. The weight-averaged molecular mass was calculated from the reduced molecular mass using the program SEDNTERP (*23*). Molecular masses determined by the global fitting were consistent with the average value obtained using the Beckman-Origin software. Several associative models for each HR1 peptide were tested using NONLIN. The simplest associative model that produced random residuals and had the lowest square root of the variance (SRV) was assumed to reflect the oligomeric state of the peptide.

Light Scattering. Multiangle light scattering measurements were obtained using a miniDAWN instrument (Wyatt Technology). The wavelength of the laser was 690 nm, and all samples were tested in microbatch mode at a concentration of 20 μM in phosphate buffer [50 mM KPO_4 and 100 mM NaCl (pH 7.0)] with buffer injections made before and after each sample. All solutions were filtered through a 0.02 μm filter (Whatman Anatop) prior to injection. UV absorbance readings of the sample were taken before and after injection to obtain an accurate sample concentration and to monitor for aggregation. Molecular masses were calculated using ASTRA 4.72 software (Wyatt Technology), assuming a d*n*/d*c* value of 0.19 mL/g.

RESULTS

Table 1 lists the peptide sequences, T_m values, and percent helicity values for a series of peptides derived from the HR1 region of gp41. Boxes are used to highlight the residues

Table 1: Peptide Sequences, Thermal Stability, and Helicity Data

Peptide[a]	Length		Tm (C) HR1 10 μM	Tm (C) HR1 +T649[b]	HR1 % helicity 10 μM
N-Terminal Truncations of HR1 region					
T865	51	QARQLLSGIVQQQNNLLRAIEAQQHLLQLTVWGIKQLQARILAVERYLKDQ	82	91	74%
N6ΔT865	45	SGIVQQQNNLLRAIEAQQHLLQLTVWGIKQLQARILAVERYLKDQ	76	76	71
N10ΔT865	41	QQQNNLLRAIEAQQHLLQLTVWGIKQLQARILAVERYLKDQ	76	63/75	78
N13ΔT865	38	NNLLRAIEAQQHLLQLTVWGIKQLQARILAVERYLKDQ	75	66/75	83
N17ΔT865	34	RAIEAQQHLLQLTVWGIKQLQARILAVERYLKDQ	45	35	59
C-Terminal Truncations of HR1 region					
T865ΔC4	47	QARQLLSGIVQQQNNLLRAIEAQQHLLQLTVWGIKQLQARILAVERY	67	87	Agg
T865ΔC9	42	QARQLLSGIVQQQNNLLRAIEAQQHLLQLTVWGIKQLQARIL	56	87	58
T1600	44	TLTVQARQLLSGIVQQQNNLLRAIEAQQHLLQLTVWGIKQLQAR	48	86	48
T1847	34	TLTVQARQLLSGIVQQQNNLLRAIEAQQHLLQLT	<10	49	25
HR2 peptide					
T649	36	WMEWDREINNYTSLIHSLIEESQNQQEKNEQELLEL	<10	–	25
Heptad repeat		a d a d a d a d a d a d a d a d			

[a] The N-terminus and C-terminus of each peptide were acetylated and amidated, respectively. The notation to the left or right of T865 in the peptide name indicates how many residues have been truncated from the N- or C-terminus of T865, respectively. [b] The mixture of 10 μM HR1 and 10 μM T649. Two T_m values are listed when two independent transitions could be identified.

Table 2: Weight-Averaged Molecular Masses[a] of HR1 Peptides Obtained by Sedimentation Equilibrium and Light Scattering

	HR1 peptide alone						HR1 complex with HR2 peptide T649			
	XLA, 10 μM	light scattering, 20 μM	XLA, 100 μM	XLA, global[b]	N^c	theoretical (4-mer)	XLA, 10 + 10 μM	light scattering, 20 + 20 μM	XLA, 100 + 100 μM	theoretical (six-helix bundle)
T865	19423	Agg[f]	23773	22857	3.9	23908	29466	31810	34275	31527
N6ΔT865[d]	18547	22223	21577	nd[g]	4.1	20988	24744	33690	25796	29337
N10ΔT865	15362	18490	18583	nd[g]	3.8	19640	26316	24455	32487	28326
N13ΔT865	15484	21189	16210	19318	3.6	18104	24525	25950	nd[g]	27174
N17ΔT865	11314	15927	13244	nd[g]	3.3	16288	Agg[f]	16013	Agg[f]	25812
T865ΔC4[e]	17936	Agg[f]	29768	nd[g]	5.4	21968	Agg[f]	Agg[f]	Agg[f]	30072
T1600	4875	Agg[f]	17205	nd[g]	3.4	20248	nd[g]	21630	19371	28782
T1847	4310	3195	4136	nd[g]	1.1	15528	17577	26870	22789[h]	25242

[a] Molecular masses are given in daltons. [b] Results from global analysis of T865 and N13ΔT865 performed with data sets of 10, 50, and 100 μM, 18 000 and 22 000 rpm, and at least two wavelengths. [c] The oligomeric state is determined by dividing the 100 μM XLA molecular mass by the molecular mass of the peptide monomer. [d] The notation to the left or right of T865 in the peptide name indicates how many residues have been truncated from the amino or carboxy terminus of T865, respectively. [e] T865ΔC9 was aggregated at 10 μM under the conditions used for light scattering and XLA analysis. [f] Aggregated. [g] Not determined. [h] The reported molecular mass is for an 80 + 80 μM mixture.

which are located in the "a" or "d" position of the heptad repeat. T865 is analogous to a peptide denoted N51 in other studies (*8*) except the N- and C-terminal ends have been acetylated and amidated, respectively. The first set of sequences in Table 1 represents N-terminal truncations of T865, and the second set shows a series of C-terminal truncations. The peptides are labeled to indicate the number of residues truncated (Δ) from either the N-terminal or C-terminal end of T865. Truncations on the C-terminal side of T865 often resulted in peptides with lower solubility and larger amounts of aggregated material, and so adjustments to the N-terminus were made to select peptides that were amenable to study. The HR2 peptide (T649) which was used to form six-helix bundles with the HR1 peptides is also given.

The weight-averaged molecular masses for each peptide obtained by analytical ultracentrifugation and light scattering are listed in Table 2. Expected molecular masses for a tetramer are also given. The oligomeric state (N) is calculated from the ratio of the observed molecular mass (determined by analytical ultracentrifugation at a peptide concentration of 100 μM) to the molecular mass of a peptide monomer. Although some peptides, particularly those with truncations to the C-terminal side, had a tendency to aggregate, the molecular mass of most HR1 oligomers approaches that of a tetramer at 100 μM. This is shown graphically in Figure 1 for T865 and N13ΔT865. At >50 μM, these peptides have molecular masses within 10% of that of a tetramer. At 250 μM, T865 begins to aggregate. At <10 μM, these peptide complexes begin to fall apart, and the less stable N13ΔT865 approaches the monomer molecular mass at 1 μM. The only peptide that was not tetrameric was T1847, which is monomeric up to 250 μM and is discussed in more detail below. Previous work has indicated that N13ΔT865 exists in a monomer−tetramer equilibrium (*25*), so the appearance of tetramers was not surprising. The weight-averaged molecular masses of T865 and N13ΔT865 at 100 μM are within 1 and 10%, respectively, of the expected molecular mass of a tetramer.

Most sedimentation data fit well to a single-ideal species model and showed no evidence of aggregation. Molecular masses labeled as "aggregated" in Table 2 did not fit the single-ideal species model well, had molecular masses that varied with rotor speed, could not be fit by an associative model, or had absorbance values which declined more than 50% during the light scattering experiment.

The formation of a soluble, self-associated complex by HR1 peptides would appear to be in contrast to previously published reports that N51 severely aggregates in solution

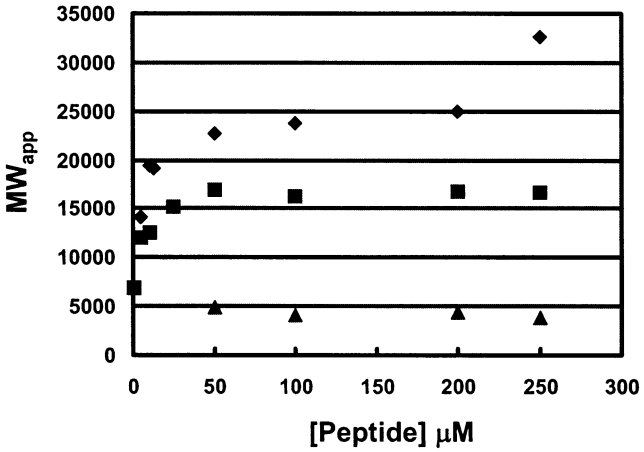

FIGURE 1: Apparent molecular mass determined as a function of loading concentration for T865 (◆), N13ΔT865 (■), and T1847 (▲). Molecular masses were determined by fitting the data at each concentration to a single-ideal species model and averaging the results from different rotor speeds and wavelengths (see Materials and Methods). The expected molecular mass for a tetramer is given in Table 2. Errors in molecular mass determinations are less than 10%.

(*8*, *26*). However, peptides synthesized with blocked termini were found to be amenable for biophysical study. Differences in HR1 sequence and sample preparation were also found to affect the degree of aggregation.

T865 Self-Associates into a Stable Helical Tetramer. Figure 2A shows the thermal stability of T865. The cooperative thermal unfolding transition, with a melting temperature (T_m) of 82 °C (Table 1), indicates that the self-associated complex of T865 forms an ordered structure. Figure 3A shows the CD spectrum for T865, which is indicative of a species that forms an α-helix. On the basis of a deconvolution of this spectrum (see Materials and Methods), this peptide was found to be 74% helical (Table 1).

Analytical ultracentrifugation data indicate that the weight-averaged molecular mass of T865 is within 1% of the expected molecular mass of a tetramer at 100 μM (Table 2). This is in agreement with the results from studies of a shorter peptide derived from the HR1 region of HIV-1 that was previously found to be tetrameric (ref *25* and N13ΔT865 presented here).

For T865 and N13ΔT865, a more detailed analysis of the analytical ultracentrifugation data was performed. Using the program NONLIN, up to 15 separate data files (spanning concentrations from 1 to 200 μM) were simultaneously fit to determine the molecular mass and the appropriate oligomeric model. The weight-averaged molecular masses (labeled "global" in Table 2) determined by this global analysis (22 857 and 19 318 Da for T865 and N13ΔT865, respectively) are consistent with the formation of tetrameric species. Several associative models were used to further confirm the oligomeric association. Table 3 contains the square root of the variance (SRV) for each model for T865 and N13ΔT865. It is evident that a model containing a tetrameric species fits these data best. For T865, models incorporating a tetrameric species (either a monomer−tetramer or monomer−dimer−tetramer species) produced the lowest SRV values

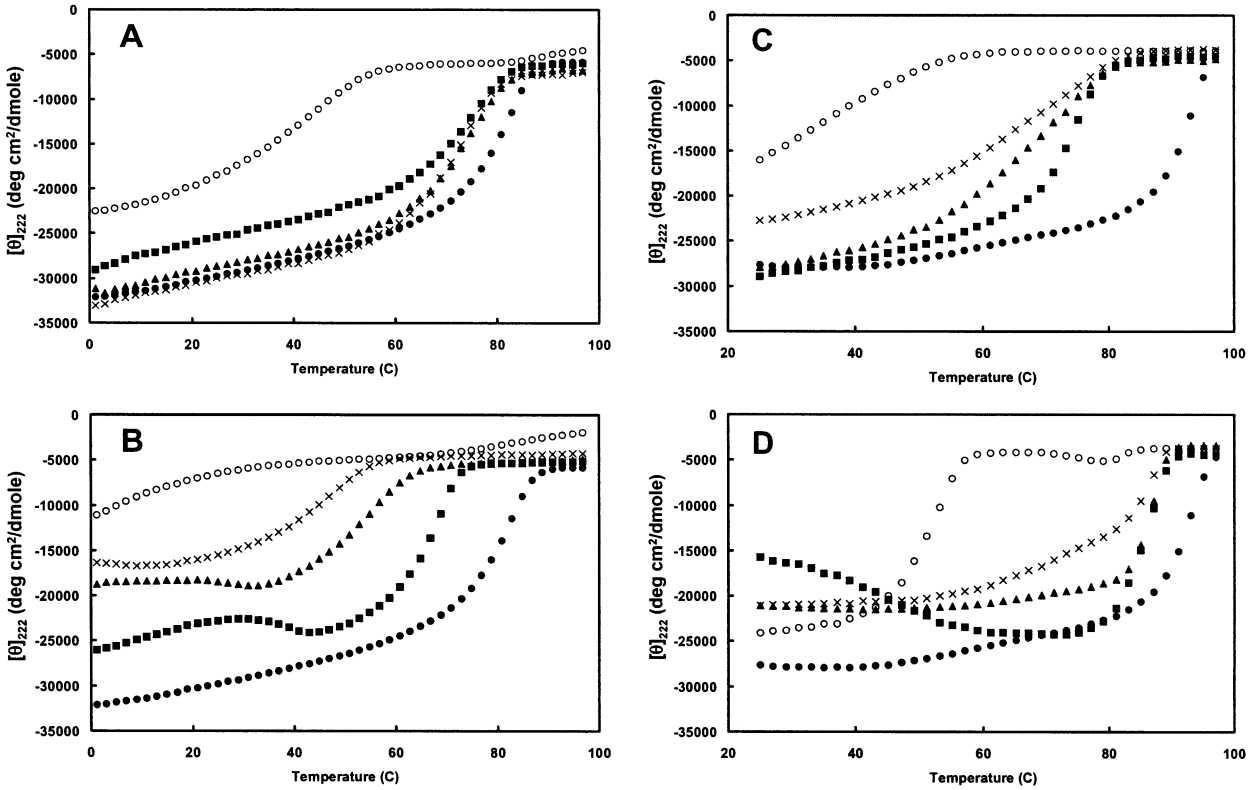

FIGURE 2: Thermal unfolding transitions of HR1 oligomers (panels A and B, peptide concentration of 10 μM) and HR1 peptides in complex with the HR2 peptide T649 (panels C and D, peptide concentrations of 10 + 10 μM) as determined by circular dichroism at 222 nm: (A) T865 (●), N6ΔT865 (■), N10ΔT865 (▲), N13ΔT865 (×), and N17ΔT865 (○), (B) T865 (●), T865ΔC4 (■), T865ΔC9 (▲), T1600 (×), and T1847 (○), (C) T649 in complex with T865 (●), N6ΔT865 (■), N10ΔT865 (▲), N13ΔT865 (×), and N17ΔT865 (○), and (D) T649 in complex with T865 (●), T865ΔC4 (■), T865ΔC9 (▲), T1600 (×), and T1847 (○). Data were collected in 50 mM KPO_4 and 100 mM NaCl (pH 7.0).

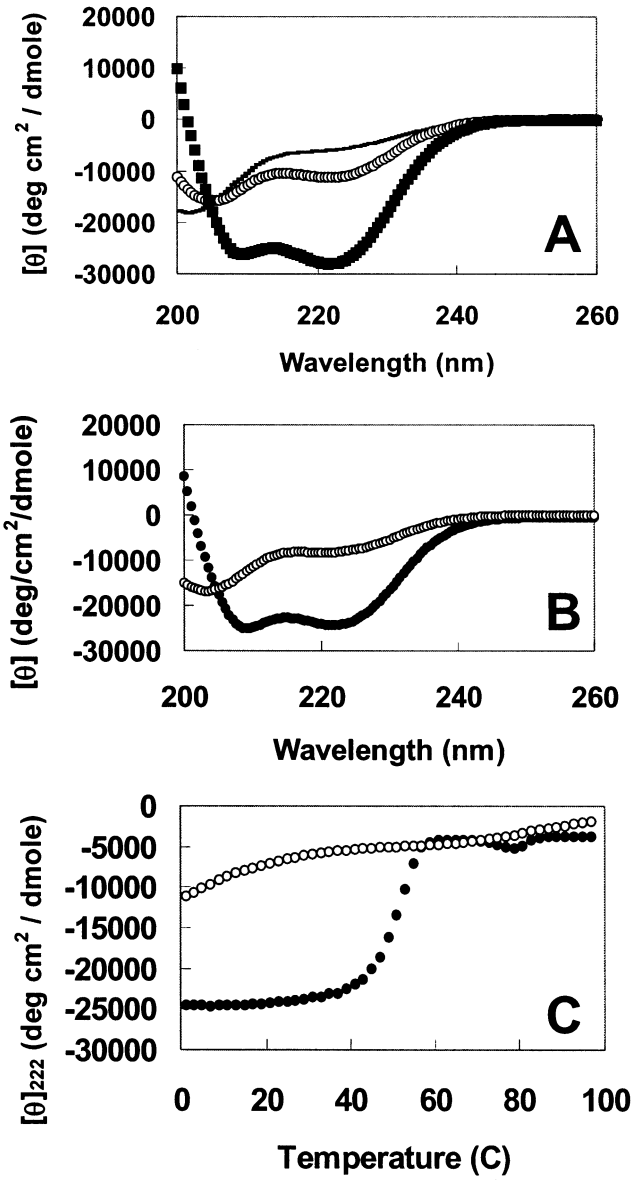

FIGURE 3: Circular dichroism spectra of (A) T865 (■), T1847 (○), and T649 (—). Spectra were collected at a peptide concentration of 10 μM in 50 mM KPO_4 and 100 mM NaCl at pH 7.0 and 4 °C. (B) Observed spectra of a mixture of 10 μM T1847 and 10 μM T649 in 50 mM KPO_4 and 100 mM NaCl at pH 7.0 and 4 °C (●) and theoretical spectra of a sum of the individual spectra from panel A assuming no interaction between T1847 and T649 (○). (C) Thermal unfolding transition of 10 μM T1847 (○) and a mixture of 10 μM T1847 and 10 μM T649 (●) measured in 50 mM KPO_4 and 100 mM NaCl at pH 7.0.

(6.57×10^{-3} and 6.28×10^{-3}, respectively). Models with trimeric species did not fit the data as well (SRV = 10.37×10^{-3} for a monomer−trimer species) or did not converge (monomer−trimer−hexamer). Similar results were obtained for N13ΔT865, as the models with tetrameric species (monomer−tetramer and monomer−dimer−tetramer) produced low SRV values (5.98×10^{-3} and 5.76×10^{-3}, respectively), while the models containing trimeric species either did not converge (monomer−trimer) or had much higher SRV values (12.6×10^{-3} for a monomer−trimer−hexamer species).

The formation of HR1 tetramers is in contrast to the trimer observed in the crystallographic structure of the HR1−HR2 complex. However, little is known about the structure of gp41 in the nonfusogenic state, specifically the structure of the HR1 region in the absence of HR2. Previous studies have suggested the possibility of tetrameric gp41−gp120 oligomers (*27*−*29*), and chimeras of HR1 peptides with maltose binding protein (*30*) and protein A (*31*) were shown to form tetramers. However, it is unclear what role, if any, a tetrameric HR1 might have in the viral fusion process. It may also be that peptides derived from the HR1 region exhibit different behavior in isolation from that which exists in the context of gp41.

Table 3: Comparison of Fits for Several Associative Models Using NONLIN

peptide	model[a]	molecular mass (Da)	SRV ($\times 10^{-3}$)[b]
T865	single	22857	7.19
	1−3		10.37
	1−4		6.57
	1−3−6		NC[c]
	1−2−4		6.28
N13ΔT865	single	19318	15.91
	1−3		NC[c]
	1−4		5.98
	1−3−6		12.6
	1−2−4		5.76

[a] Details of the global analysis are contained in the footnotes of Table 2. [b] SRV is the square root of the variance of the fit. [c] NC denotes a calculation that did not converge.

Self-Association of T865 Is Insensitive to N-Terminal Truncation. N-Terminal truncations of T865 were made to evaluate the contribution of this region to the oligomerization of T865. Figure 2A shows the thermal unfolding transitions for these peptide oligomers. Surprisingly, truncation of up to 13 residues from the amino-terminal end of T865 (N13ΔT865) has little effect on the stability or helicity of the self-associated complex. The truncation of QARQLL has the greatest effect (6 °C), while the additional loss of SGIVQQQ has no further effect on HR1 complex stability (Table 1). These truncations include four "a" or "d" residues from the heptad repeat which are part of the hydrophobic core of the oligomer. However, truncation of four additional N-terminal residues (N17ΔT865) is more deleterious, as indicated by a T_m of 45 °C. The loss of these four residues (NNLL) results in a decrease of 30 °C in the thermal stability and 24% less helicity than in the N13ΔT865 oligomer.

All of the peptides in the set of N-terminal truncations had molecular masses approaching that of a tetramer at 100 μM and helicity values consistent with the formation of an ordered, helical structure. The observation that the level of the oligomerization state (N) at 100 μM declines as the N-terminus is truncated is likely a result of the loss of stability of the oligomeric complex, resulting in a monomer−tetramer equilibrium for the shorter peptides.

Self-Association of T865 Is Very Sensitive to Changes near the Hydrophobic Pocket. In contrast to the minimal impact of N-terminal truncation on T865 self-association, modification on the carboxy end has a profound effect on stability (Figure 2B and Table 1). Truncation of the last four amino acids on the carboxy side of T865 (T865ΔC4) reduces the T_m of the self-associated complex by 15 °C, and further truncation (AVERYLKDQ) results in a peptide (T865ΔC9) that is by 26 °C less stable than T865. These data agree with

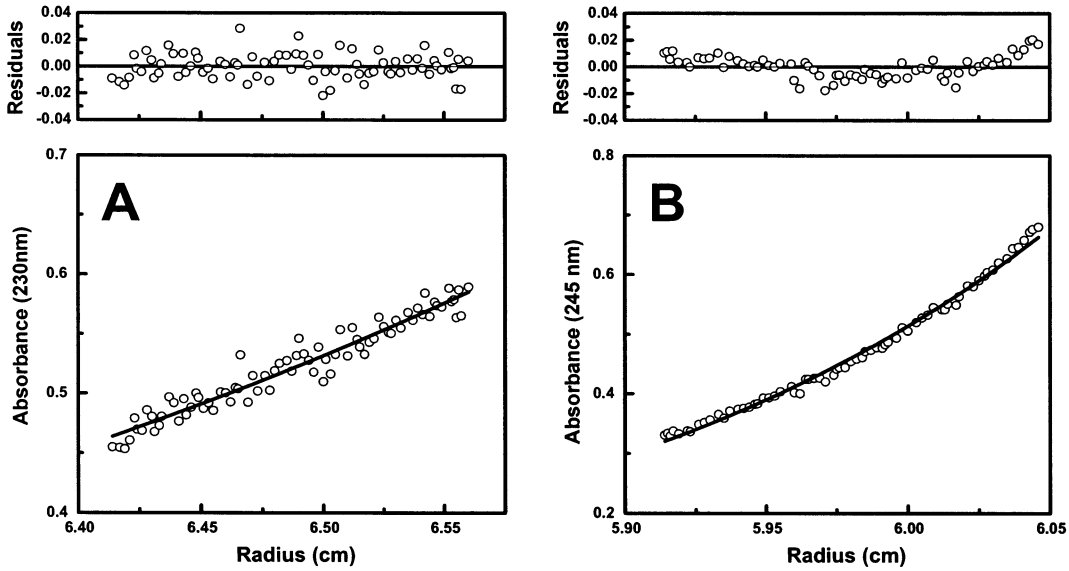

FIGURE 4: Sedimentation equilibrium results for (A) 100 μM T1847 (35 000 rpm) and (B) a mixture of 80 μM T1847 and 80 μM T649 (22 000 rpm). Lines through the data represent fits using a single-ideal species model. The weight-averaged molecular masses resulting from these analyses are 4136 Da for 100 μM T1847 and 22 789 Da for the mixture of 80 μM T1847 with 80 μM T649.

previous work showing that a 34-residue HR1 peptide (N34), which corresponds to the truncation of 11 C-terminal residues from N6ΔT865, has a T_m of approximately 40 °C (*32*) compared to a T_m of 75 °C for N6ΔT865. At <50 °C, T865ΔC4 and T865ΔC9 have unusual thermal transitions; in particular, it appears these peptides exhibit an increase in helicity prior to the unfolding transition. This is likely a result of soluble aggregates which go fully into solution prior to unfolding. Sedimentation equilibrium and light scattering clearly indicate aggregation for these peptides below 25 °C. Despite the presence of aggregates, the thermal unfolding transitions for these peptides were quite reproducible.

Further truncation of the C-terminus consistently yielded insoluble peptides. In the course of these studies, it was found that extension of the amino terminus by four residues (TLTV) substantially improved the solubility of these C-terminal truncations. Following this strategy, it was possible to study the behavior of an HR1 peptide (T1600) with 11 residues truncated (ILAVERYLKDQ) from the C-terminus. T1600 is significantly less stable than T865 (T_m = 48 °C) and only 48% helical, suggesting a substantial destabilization of helical structure.

Truncation of the Deep Pocket Abolishes Self-Association. Further truncation from the carboxy end of T865 results in a peptide (T1847) that has no discernible unfolding transition (Figure 2B). Sedimentation equilibrium experiments indicated that this peptide is monomeric up to 250 μM (Table 2 and Figure 1), and the CD spectrum indicates the peptide is 25% helical (Figure 3A and Table 1). A representative sedimentation equilibrium trace for 100 μM T1847 at 35 000 rpm is shown in Figure 4A. The single-ideal species model fit the data well, and the weight-averaged molecular mass, 4136 Da, corresponds closely to the monomer molecular mass (Table 2). Since T1847 is missing most of the residues that constitute the hydrophobic pocket [identified by the crystallographic structure of the six-helix bundle (*15*)] and does not self-associate, the pocket region of the HR1 domain seems particularly important for forming the self-associated complex. Comparison of T1847 with T1600 shows that the truncation of 10 residues in the pocket region (VWGIKQLQAR) results in a more than 30 °C drop in thermal stability. Loss of the pocket region and the last 11 residues (ILAVERYLKDQ) reduces the thermal stability by more than 70 °C.

HR1−HR2 Peptides Form Six-Helix Bundles. Elastic light scattering and analytical ultracentrifugation were used to determine the weight-average molecular masses of the complex resulting from an equimolar mixture of each HR1 peptide and the HR2 peptide T649. Table 2 lists the observed molecular masses for the complex, along with the theoretical molecular mass of a six-helix bundle. The molecular masses of these species are consistent with the formation of a six-helix bundle of three HR1 peptides and three HR2 peptides. Light scattering experiments performed at varying molar ratios of HR2 to HR1 confirm this stoichiometry (data not shown).

N-Terminal Truncation Reduces the Stability of HR1−HR2 Complexes. Peptide T649 is derived from the HR2 region of gp41 (Table 1) and has been shown by X-ray crystallography to make contacts within the hydrophobic pocket and with the amino-terminal side of the HR1 oligomer (*3*, *9*). Panels C and D of Figure 2 show the thermal unfolding transitions for the truncated HR1 peptides in complex with T649 at 10 μM each. The thermal stability of T865 in complex with T649 is 91 °C or 9 °C higher than that of the self-associated T865 oligomer (Table 1). As the N-terminus of T865 is truncated, the stability of the HR1−HR2 complex decreases significantly, as shown in Figure 2C. Truncation of the first six residues (QARQLL) from the amino terminus (N6ΔT865) reduces the stability of the complex by 15 °C. Further truncation (N10ΔT865) results in CD thermal melts with two discernible transitions revealed by the derivative of the transition curve (Figure 5). The transition in the lower 60 °C range is likely the dissociation of the HR2 peptide, while the other transition (near 75 °C) most likely corresponds to the unfolding of the self-associated HR1 complex in the absence of HR2. Similar results are obtained for the N13ΔT865 peptide (Table 1). Therefore, N-terminal trunca-

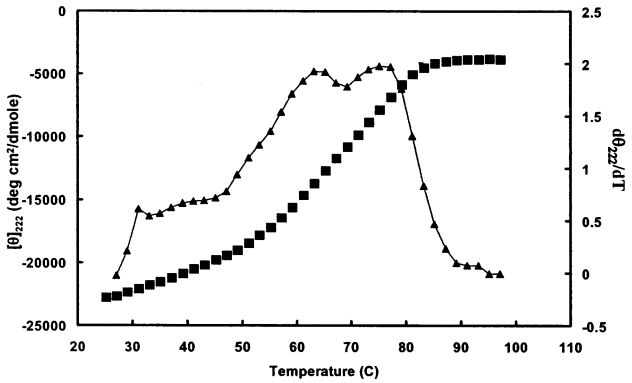

FIGURE 5: Determination of T_m for oligomeric complexes. The thermal unfolding transition (■) for a mixture of 10 μM N10ΔT865 and 10 μM T649 is plotted on the left axis, and the derivative of this curve (dθ/dT) is shown on the right axis (▲). In this example, two distinct maxima are observed. One is at 63 °C, which likely represents the dissociation of T649, and the other is at 75 °C, which is identical to the T_m for the HR1 tetramer.

tion of up to 13 residues of T865 results in an HR1−HR2 complex that has a melting transition up to 30 °C lower than that of the T865−T649 complex. The binding of T649 to N17ΔT865 is very weak (the T_m is 56 °C lower than that of the T865−T649 complex), presumably because the majority of the HR2 binding epitope has been removed.

C-Terminal Truncations Form Stable HR1−HR2 Complexes. The HR2 peptide T649 forms stable complexes with C-terminal truncations of T865, despite the marked reduction in the structural stability of the HR1 oligomer. Figure 2D presents the thermal unfolding transitions, and Table 1 lists the corresponding T_m values for these complexes. These data reveal complex stabilities comparable to those obtained for the T865−T649 complex. For example, the T865ΔC9−T649 complex has a T_m of 87 °C, compared to a T_m of 91 °C for the T865−T649 complex. Even in the case of T1847, which is monomeric and nonhelical, a stable six-helix bundle (T_m = 49 °C) was still formed with T649.

Interaction between T1847 and T649. The CD spectra of T1847 and T649 (Figure 3A) demonstrate that these peptides have little intrinsic α-helical structure by themselves. The CD spectrum of the mixture of T1847 and T649 (Figure 3B) is significantly more helical than the sum of the individual spectra, suggesting that the addition of T649 induces helical structure in both peptides. Helicity calculations on the T1847−T649 complex reveal that the peptides are 70% helical. The thermal unfolding transitions of T1847 and the T1847−T649 complex are shown in Figure 3C. T1847 has a nearly featureless melt, demonstrating that this peptide does not form a cooperative oligomeric complex. A similar temperature dependence is also observed for the HR2 peptide T649 (data not shown). Addition of stoichiometric amounts of T649 to T1847 results in a CD melt with a sharp transition and a midpoint of 49 °C. Figure 4B shows the sedimentation equilibrium analysis for a mixture of T1847 and T649 (80 μM each) at 22 000 rpm. The single-ideal species model indicates a molecular mass of 22 789 Da, which approaches that expected for a six-helix bundle (Table 2). To our knowledge, this is the first observation of a monomer to six-helix bundle transition in models of HIV gp41.

DISCUSSION

Models of gp41 oligomerization have proven to be useful tools for structure function analysis of viral fusion. However, many of these models consist of either chimeras of HR1 and fusion proteins (*30*, *31*) or trimeric proteins such as GCN4 (*33*), or single-chain constructs with the HR1 and HR2 domains separated by a flexible linker (*34*, *35*). Therefore, the contributions by specific residues toward HR1 self-assembly cannot be parsed out easily. In the work presented here, we have used truncated versions of an HR1-derived peptide, T865, to systematically study HR1 oligomerization and to identify regions that stabilize the HR1 self-associated complex.

Although T865 has the highest T_m (82 °C) of the peptides studied, it is only 7 °C more stable than N13ΔT865 and is nearly 10% less helical. Evidently, these 13 residues, which include four core "a" and "d" positions, do not contribute greatly to the stability of the HR1 self-associated complex. In the peptide model used here, these residues may be less structured than residues in the vicinity of the deep pocket and may only form the coiled-coil core in the presence of an HR2 peptide. This notion is supported by the monomeric behavior of T1847, which contains the putative disordered region but lacks most of the deep pocket. The ability of T1847 to form a stable six-helix bundle was unexpected and demonstrates that the HR2 peptide can induce the formation of the HR1 core.

Given the relative insensitivity to truncation on the N-terminal side of T865, the loss of stability observed in T1847 is rather striking. These data suggest that the last 15−20 amino acids of T865 are the central binding domain or "trigger sequence" for the self-association of peptides derived from the HR1 region of gp41. Such trigger sequences have been identified in other coiled coils and have been shown to be essential for proper oligomerization (*36*, *37*).

T1847 was one of the most interesting peptides in this series since this monomeric peptide retained the ability to bind to T649. T1847 lacks nearly all of the deep pocket residues and was found to be monomeric in solution up to concentrations more than 10 times higher (250 μM) than that required for self-association of the other HR1 peptides. However, T1847 can still form a relatively stable (T_m = 49 °C) six-helix bundle structure with T649. This suggests that HR2 regions may have the ability to direct six-helix bundle assembly in the absence of a preformed HR1 oligomeric complex. The interaction with the monomeric T1847 is presumably because nearly all HR2 contacts are present, and so it becomes energetically favorable to form the complex. Even though stable six-helix bundles can be formed without the deep pocket, this region seems to be uniquely important in stabilizing the HR1 self-associated complex and for the formation of a high-affinity HR1−HR2 complex. Since the deep pocket region is highly conserved in HIV (*38*, *39*) and is very sensitive to mutation (*40*, *41*), it is tempting to speculate that the contributions by the deep pocket region to HR1 self-association may have significance in the process of viral fusion.

Analogous Contributions in the HR1 Domain of the RSV F-Protein. It has been shown in our lab that portions of HR1 peptides derived from the respiratory syncitial virus (RSV) F1 subunit preferentially affect the stability of the self-

associated HR1 complex (*19*). The crystallographic structure of the RSV HR1−HR2 complex has been subsequently determined (*18*), and a hydrophobic pocket, analogous to the pocket in gp41, was identified. Therefore, the contribution by this groove to the structural stability of the HR1 oligomeric complex can be made for RSV. In the HR1 peptides from RSV (*19*), the hydrophobic pocket was again located on the C-terminal end of the peptide. It is striking that removal of just four residues on the C-terminal end of the RSV HR1 peptide (Figure 1B of ref *19*) results in a greater than 60 °C drop in the thermal stability of the HR1 self-associated complex (a trimeric species in the case of RSV). These residues are located precisely in the hydrophobic pocket and suggest that in both RSV and HIV, residues in this region can significantly stabilize the self-associated complex. As for HIV, truncation on the N-terminal side of the pocket was less deleterious. For example, truncation of seven residues reduces the transition temperature by only 11−13 °C (*19*). Similar results are also observed for the analogous HR1 region of human parainfluenza virus III (M. K. Delmedico, unpublished experiments). For each of these viruses, there appears to be a hot spot of binding energy in the coiled-coil HR1 oligomer that is located in a region forming a hydrophobic groove known to be important for the binding of HR2 peptides. It may be that this region is part of a conserved mechanism for stabilizing the oligomeric inner core of viral fusion proteins.

The localization of binding energy observed in HIV gp41 and the RSV F1 protein is reminiscent of energetic hot spots found in many protein−protein interfaces (*42*). In human growth hormone (hGH), for example, it was found that despite extensive contacts between the hormone and the hGH receptor, the majority of the interaction energy was contained in just a few key residues (*43*, *44*). These contacts not only produce high affinity between binding partners but also may introduce structural specificity. Therefore, the energetic importance of the deep pocket may also be reflecting a specific requirement for proper gp41 oligomerization in the virus.

Interestingly, the crystal structure of the RSV HR1−HR2 complex also resolves the unusual importance of the C-terminal leucine in our previous study (*19*). The stuttering of the 3−4 repeat observed at the C-terminal end of the HR1 peptide in the crystal structure makes this leucine a core residue, providing close packing contacts within the center of the trimeric coiled coil much like an "a" or "d" residue would. Therefore, some portion of the 11−13 °C drop in the transition temperature upon the removal of this single leucine reflects the loss of these packing contacts. It is also interesting that this residue is in the region that forms the hydrophobic pocket, which may further explain the unusual importance of this residue.

Implications for Viral Fusion. In the current model of viral fusion, it is thought that the HR1 domain oligomerizes first, followed by the interaction of HR2 just prior to fusion. Stabilization of the HR1 core by the deep pocket may serve to better orient the HR2 binding epitope on the HR1 oligomeric complex. Site-directed mutagenesis in HIV also implicates the HR1 region as being essential for fusion (*35*, *40*, *41*, *45*). Mutations at numerous locations along HR1 result in phenotypes that are unable to form syncitia even though the fusion proteins are processed correctly and can be incorporated into the virion. These data support the notion that structural elements have an important role in the strong conservation of the HR1 region (*38*, *39*). Although some of this conservation is due to other factors, such as interactions with cell surface receptors or other cofactors, it has been demonstrated that there is a relationship between the structural stability of the gp41 complex and the ability of the intact glycoprotein to undergo membrane fusion (*35*, *45*). This report demonstrates the structural importance of a small (∼15-amino acid) region around the hydrophobic pocket for HR1 self-association in HIV gp41. The unusual behavior of T1847, exhibiting a monomer to hexamer transition in the presence of the HR2 peptide T649, even offers the possibility that the HR1 region of gp41 need not oligomerize prior to the interaction of the HR2 domain. It is also interesting that the N-terminal region of T865, where the stability of the HR1 complex is less sensitive to truncation, is also the region of the virus that mutates in the development of *in vitro* resistance to HR2-derived peptide therapeutics (*16*). These results seem complementary, and suggest that there may be a higher degree of structural plasticity in this region of gp41. Further structure−function studies in this region will be required to understand the structural transition from the native to the fusogenic state.

Applicability to Other Coiled-Coil Structures. Several studies of coiled coils in general (*13*), and gp41 in particular (*46*), have demonstrated the importance of core "a" and "d" positions to structural stability. It has also been shown that polar residues in the "a" or "d" positions can influence the size of cavities within the trimeric coiled-coil core of GCN4 (*47*). Furthermore, short trigger sequences in coiled-coil peptides have been shown to be critical for proper oligomerization (*37*) in much the same way the deep pocket region is required for HR1 oligomerization. Taken together, it is becoming clear that the coiled-coil motif can exhibit an exquisite degree of specificity. In this work, we have demonstrated that specific regions of the HR1 domain of gp41 make significant contributions to the stability of the self-associated complex while others, possessing similar core residues, do not. These results suggest that coiled-coil interactions may not have a homogeneous distribution of contact in the "a"−"d" core, but rather consist of energetic hot spots. These regions may represent structural elements that could be targeted by small molecule inhibitors in the same way that the hydrophobic pocket has been shown to be an attractive antiviral target (*15*, *17*, *48*). With the results presented here, a region of gp41 has been identified that may be an attractive target for preventing HR1 oligomerization, which is thought to represent an earlier step in the viral fusion process. Since coiled-coil motifs appear in many critical biological systems, such as in gene regulation, vesicle fusion, and apoptosis (*49*, *50*), identifying hot spots in coiled-coil proteins should help in the understanding of the structural determinants of oligomerization and may prove to be a useful drug design strategy.

ACKNOWLEDGMENT

We thank Reagan Greene and Larry Stoltenberg for synthesis and purification of peptides used in this work, Dennis Lambert for many helpful discussions, and Dani Bolognesi for his continued support.

REFERENCES

1. Weissenhorn, W., Dessen, A., Calder, L. J., Harrison, S. C., Skehel, J. J., and Wiley, D. C. (1999) *Mol. Membr. Biol. 16*, 3−9.
2. Helseth, E., Olshevsky, U., Furman, C., and Sodroski, J. (1991) *J. Virol. 65*, 2119−2123.
3. Chan, D. C., Fass, D., Berger, J. M., and Kim, P. S. (1997) *Cell 89*, 263−273.
4. Chan, D. C., and Kim, P. S. (1998) *Cell 93*, 681−684.
5. Kilby, J. M., Hopkins, S., Venetta, T. M., DiMassimo, B., Cloud, G. A., Lee, J. Y., Alldredge, L., Hunter, E., Lambert, D., Bolognesi, D., Matthews, T., Johnson, M. R., Nowak, M. A., Shaw, G. M., and Saag, M. S. (1998) *Nat. Med. 4*, 1302−1307.
6. Wild, C. T., Shugars, D. C., Greenwell, T. K., McDanal, C. B., and Matthews, T. J. (1994) *Proc. Natl. Acad. Sci. U.S.A. 91*, 9770−9774.
7. Wild, C., Dubay, J. W., Greenwell, T., Baird, T., Jr., Oas, T. G., McDanal, C., Hunter, E., and Matthews, T. (1994) *Proc. Natl. Acad. Sci. U.S.A. 91*, 12676−12680.
8. Lu, M., Blacklow, S. C., and Kim, P. S. (1995) *Nat. Struct. Biol. 2*, 1075−1082.
9. Weissenhorn, W., Dessen, A., Harrison, S. C., Skehel, J. J., and Wiley, D. C. (1997) *Nature 387*, 426−430.
10. Delwart, E. L., Mosialos, G., and Gilmore, T. (1990) *AIDS Res. Hum. Retroviruses 6*, 703−706.
11. Gallaher, W. R., Ball, J. M., Garry, R. F., Griffin, M. C., and Montelaro, R. C. (1989) *AIDS Res. Hum. Retroviruses 5*, 431−440.
12. Chambers, P., Pringle, C. R., and Easton, A. J. (1990) *J. Gen. Virol. 71*, 3075−3080.
13. Harbury, P. B., Zhang, T., Kim, P. S., and Alber, T. (1993) *Science 262*, 1401−1407.
14. Bryson, J. W., Betz, S. F., Lu, H. S., Suich, D. J., Zhou, H. X., O'Neil, K. T., and DeGrado, W. F. (1995) *Science 270*, 935−941.
15. Chan, D. C., Chutkowski, C. T., and Kim, P. S. (1998) *Proc. Natl. Acad. Sci. U.S.A. 95*, 15613−15617.
16. Rimsky, L. T., Shugars, D. C., and Matthews, T. J. (1998) *J. Virol. 72*, 986−993.
17. Eckert, D. M., Malashkevich, V. N., Hong, L. H., Carr, P. A., and Kim, P. S. (1999) *Cell 99*, 103−115.
18. Zhao, X., Singh, M., Malashkevich, V. N., and Kim, P. S. (2000) *Proc. Natl. Acad. Sci. U.S.A. 97*, 14172−14177.
19. Lawless-Delmedico, M. K., Sista, P., Sen, R., Moore, N. C., Antczak, J. B., White, J. M., Greene, R. J., Leanza, K. C., Matthews, T. J., and Lambert, D. M. (2000) *Biochemistry 39*, 11684−11695.
20. Edelhoch, H. (1967) *Biochemistry 6*, 1948−1954.
21. Cantor, C. R., and Schimmel, P. R. (1980) *Biophysical Chemistry Part II: Techniques for the Study of Biological Structure and Function*, W. H. Freeman and Co., New York.
22. Johnson, J., and Curtis, W. (1990) *Proteins: Struct., Funct., Genet. 7*, 205−214.
23. Laue, T. M., Shah, B. D., Ridgeway, T. M., and Pelletier, S. L. (1992) *Analytical Ultracentrifugation in Biochemistry and Polymer Science*, The Royal Society of Chemistry, Cambridge, U.K.
24. Johnson, M. L., Correia, J. A., Halvorson, H. R., and Yphantis, D. A. (1981) *Biophys. J. 36*, 575−588.
25. Lawless, M. K., Barney, S., Guthrie, K. I., Bucy, T. B., Petteway, S. R., Jr., and Merutka, G. (1996) *Biochemistry 35*, 13697−13708.
26. Blacklow, S. C., Lu, M., and Kim, P. S. (1995) *Biochemistry 34*, 14955−14962.
27. Pinter, A., Honnen, W., Tilley, S. A., Bona, C., Zaghouani, H., Gorny, M., and Zolla-Pazner, S. (1989) *J. Virol. 63*, 2674−2679.
28. Earl, P. L., Doms, R. W., and Moss, B. (1990) *Proc. Natl. Acad. Sci. U.S.A. 87*, 648−652.
29. Thomas, D. J., Wall, J. S., Hainfeld, J. F., Kaczorek, M., Booy, F. P., Trus, B. L., Eiserling, F. A., and Steven, A. C. (1991) *J. Virol. 65*, 3797−3803.
30. Shugars, D. C., Wild, C. T., Greenwell, T. K., and Matthews, T. J. (1996) *J. Virol. 70*, 2982−2991.
31. Bernstein, H. B., Tucker, S. P., Kar, S. R., McPherson, S. A., McPherson, D. T., Dubay, J. W., Lebowitz, J., Compans, R. W., and Hunter, E. (1995) *J. Virol. 69*, 2745−2750.
32. Lu, M., and Kim, P. S. (1997) *J. Biomol. Struct. Dyn. 15*, 465−471.
33. Shu, W., Ji, H., and Lu, M. (1999) *Biochemistry 38*, 5378−5385.
34. Tan, K., Liu, J., Wang, J., Shen, S., and Lu, M. (1997) *Proc. Natl. Acad. Sci. U.S.A. 94*, 12303−12308.
35. Liu, J., Shu, W., Fagan, M. B., Nunberg, J. H., and Lu, M. (2001) *Biochemistry 40*, 2797−2807.
36. Kammerer, R. A., Schulthess, T., Landwehr, R., Lustig, A., Engel, J., Aebi, U., and Steinmetz, M. O. (1998) *Proc. Natl. Acad. Sci. U.S.A. 95*, 13419−13424.
37. Frank, S., Lustig, A., Schulthess, T., Engel, J., and Kammerer, R. (2000) *J. Biol. Chem. 275*, 11672−11677.
38. Delwart, E. J., Mosialos, G., and Gilmore, T. (1990) *AIDS Res. Hum. Retroviruses 6*, 703−706.
39. Dong, X.-N., Xiao, Y., Dierich, M. P., and Chen, Y.-H. (2001) *Immunol. Lett. 75*, 215−220.
40. Cao, J., Bergeron, L., Helseth, E., Thali, M., Repke, H., and Sodroski, J. (1993) *J. Virol. 67*, 2747−2755.
41. Weng, Y., Yang, Z., and Weiss, C. D. (2000) *J. Virol. 74*, 5368−5372.
42. Bogan, A. A., and Thorn, K. S. (1998) *J. Mol. Biol. 280*, 1−9.
43. Cunningham, B. C., and Wells, J. A. (1989) *Science 244*, 1081−1085.
44. Cunningham, B. C., and Wells, J. A. (1993) *J. Mol. Biol. 234*, 554−563.
45. Lu, M., Ji, H., and Shen, S. (1999) *J. Virol. 73*, 4433−4438.
46. Shu, W., Liu, J., Ji, H., Radigen, L., Jiang, S., and Lu, M. (2000) *Biochemistry 39*, 1634−1642.
47. Akey, D. L., Malashkevich, V. N., and Kim, P. S. (2001) *Biochemistry 40*, 6352−6360.
48. Ferrar, M., Kapoor, T. M., Strassmaier, T., Weissenhorn, W., Skehel, J. J., Oprian, D., Schreiber, S. L., Wiley, D. C., and Harrison, S. C. (1999) *Nat. Struct. Biol. 6*, 953−960.
49. Burkhard, P., Stetefeld, J., and Strelkov, S. (2001) *Trends Cell Biol. 11*, 82−88.
50. Weber, T., Zemelman, B. V., McNew, J. A., Westerman, B., Gmachl, M., Parlati, F., Sollner, T. H., and Rothman, J. E. (1998) *Cell 92*, 759−772.

BI027283N